Electronic Supplementary Material (ESI) for Journal of Materials Chemistry A.

Supporting Information

Selective dye adsorption and metal ion detection using multifunctional silsesquioxane-based tetraphenylethene-linked nanoporous polymer with high surface area and bimodal structure

Huanhuan Liu[a], Hongzhi Liu[a,b,c]*

a.Key Laboratory of Special Functional Aggregated Materials, Ministry of Education, School of Chemistry and Chemical Engineering,Shandong University, Jinan, 250100, P. R. China

b. Key Laboratory of Organosilicon Chemistry and Material Technology of Ministry of Education, Hangzhou Normal University，Hangzhou 31112, P. R. China.

c. Wuxi Detan Technology Co., Ltd, No. 588 Jinhui Rd. Huishan District, Wuxi, Jiangsu (China)

**Corresponding Author, E-mail: liuhongzhi@sdu.edu.cn*

Experimental Section

Methods

Fourier-transform infrared (FTIR) spectra were recorded with a Bruker Tensor 27 spectrophotometer with a disc of KBr from 4000 to 400 cm^{-1} at a resolution of 4 cm^{-1}. The data were treated with OPUS spectroscopy software version 6. Solution-state ^{1}H NMR spectrum was measured with a Bruker Avance 300 spectrometer, and solution-state ^{13}C NMR spectrum was recorded with a Bruker Avance 400 spectrometer in $CDCl_3$ with tetramethylsilane as the internal standard. The resonance frequencies were 300 MHz for ^{1}H NMR, 100 MHz for ^{13}C NMR spectroscopy.

Solid-state ^{13}C cross-polarization/magic-angle-spinning (CP/MAS) NMR and ^{29}Si MAS NMR spectra were performed with a Bruker Avance-500 NMR spectrometer operating at a magnetic field strength of 9.4 T. The resonance frequencies were 125 and 99 MHz for ^{13}C NMR and ^{29}Si NMR, respectively. A chemagnetics 5 mm triple-resonance MAS probe was used to acquire ^{13}C

NMR and ^{29}Si NMR spectra. ^{29}Si MAS NMR spectra with high-power proton decoupling were recorded by using a $\pi/2$ pulse length of 5 μs, a recycle delay of 120 s, and a spinning rate of 5 kHz. Powder X-ray diffraction (PXRD) was measured with a Riguku D/MAX 2550 diffractometer under Cu-K_{α} radiation, 40 kV, 200 mA with a 2θ range of 5-80° (scanning rate of $10°\text{min}^{-1}$) at room temperature.

Nitrogen adsorption-desorption isotherm measurements were performed with a QuadraSorb SI apparatus at 77 K. The samples were degassed at 150 °C for 12 h prior to measurement. A sample of ca. 100 mg and UHP-grade nitrogen (99.999%) gas source were used in the nitrogen sorption measurements and collected with a Quantachrome Quadrasorb apparatus. BET surface areas were evaluated over a P/P_0 range from 0.01 to 0.20. Nonlocal density functional theory (NL-DFT) pore-size distributions were confirmed by using the carbon/slit-cylindrical pore mode of the Quadrawin software. CO2 adsorption isotherms were measured with Micromeritics TriStar II3020V1.04. Before the measurement, the samples were degassed at 120 °C under vacuum for at least 12 h.

Thermogravimetric analyses (TGA) were conducted with a Mettler-Toledo SDTA-854 TGA system in nitrogen (100 mL min^{-1}) at a heating rate of 10 °C min^{-1} from temperature to 800 °C. Elemental analyses were performed with an Elementar EL III elemental analyzer. High-resolution transmission electron microscopy (HR-TEM) experiments were recorded with a JEM 2100 electron microscope (JEOL, Japan) with an acceleration voltage of 200 kV. Field-emission scanning electron microscopy (FE-SEM) experiments were recorded with a HITACHI S4800 spectrometer. UV-vis adsorption spectra of organic dyes were collected on an a TU-1901 double beam UV-vis spectrophotometer. The luminescence excitation spectra were measured on Hitachi F-4500 fluorescence spectrophotometer equipment.

Dye adsorption experiments

Adsorption kinetics

The bath mode adsorption studies for various dyes, including Rhodamine B (RB), Methylene blue (MB)，Methyl orange (MO),Congo red (CR), Crystal violet (CV) were carried out. In the process, all dyes were dissolved in deionized water and 0.01 g of HPP-3 were added to 30 mL of dye solution with different concentration. The mixture was stirred at room temperature for 24 h until the equilibrium was reached. The concentration of dye solutions before and after adsorption was determined by a Ultraviolet-visible(UV-vis) spectrophotometer.

$$Q_e = \frac{(C_0 - C_e)\cdot V}{m} \qquad Q_t = \frac{(C_0 - C_t)\cdot V}{m}$$

Where m(g) represents the mass of HPP-3 and V（mL）is the volume of RB, MB, CR or MO solution. C_0 and C_t (mg L^{-1}) are the initial and final (post-adsorption) concentrations of the dye solutions, respectively.

Adsorption isotherms and relevant parameters are usually used to determine the adsorption mechanism. The obtained equilibrium adsorption data can be analyzed by fitting against the langmuir and freundlich isotherm models (Equation 1 and 2),

$$\frac{C_e}{Q_e} = \frac{1}{Q_m} \cdot K_L + \frac{1}{Q_m} \cdot C_e$$ Langmuir model

$$\ln Q_e = \ln K_F + \frac{1}{n} \cdot \ln C_e$$ Freundlich model

Where K_L (L mg^{-1}) and Q_m (mg g$^{-1)}$ represent Langmuir constant and the maximum adsorption capacity calculated by Langmuir model, respectively. K_F and 1/n are Freundlich constants that describe the adsorption capacity and intensity, respectively.

Adsorption kinetic are of great importance in the adsorption process as they can predict the removal rate of certain pollutants from aqueous solutions and help get a better understanding of the adsorption mechanism. The pseudo-second-order, pseudo-first-order and intraparticle diffusion models were used to simulate the adsorption kinetics in this research and the linear from of the pseudo-second-order can be expressed as the following equation

$$\ln(q_e - q_t) = \ln q_e - k_1 \cdot t$$ The pseudo-first order model

$$\frac{t}{q_t} = \frac{1}{k_2 \cdot q_e^2} + \frac{t}{q_e}$$ The pseudo-second order model

$$q_t = k_i \cdot t^{0.5}$$ Intraparticle diffusion model

Where q_e and q_t refer to the adsorption capacity at equilibrium and at time t (min); k_1 (min^{-1}), k_2 (g mg^{-1}min^{-1}) and k_i (mg g^{-1} min$^{-0.5}$) are the adsorption rate constants for the pseudo-first-order, pseudo second-order, and intraparticle diffusion models, respectively.

Adsorption selectivity

In the process, 0.01 g of HPP-3 were added to 30 mL of Rhodamine B (RB) - Methylene blue (MB), Rhodamine B (RB) - Methyl orange (MO), rhodamine B (RB) - Methylene blue (MB) - Crystal violet (CV) solutions with initial concentration was 40 mg L^{-1}. Then, after adsorption equilibrium, the absorbance of RB, MB, MO and CV was measured at 554, 665, 466, 586 and 497 nm, respectively. The removal efficiency of the dye (E) was calculated using formula.

$$E(\%) = \frac{C_0 - C_e}{C_0} \times 100$$

Where C_0 and C_e are the initial and equilibrium concentration of the dye (mg L^{-1}), respectively.

Preparation of metal-ion solutions

To examine the potential of the HPPs for sensing metal ions, metal ions are dissolved in anhydrous ethanol and 3 mg HPP-3 was added to 10 mL ethanol solutions (the metal ion concentration is 10^{-3} mol L^{-1}) including Fe^{3+}、Cu^{2+}、Ru^{3+}、Zn^{2+}、Li^{+}、Mn^{2+}、Co^{2+}、Pb^{2+}、Sn^{4+}、Al^{3+} and Ni^{2+} to form the metal ion incorporated HPPs suspension for luminescence studies. The excitation wavelength is 350 nm and the voltage is 700 V. The widths of the excitation slit are 5 nm and emission slit is 5 nm for the HPP-3. The stock solutions were diluted to the desired concentrations for further experiments.

Table of Contents

Table S1 Elemental analysis of HPPs

Sample	Experimental Value		Theoretical Value	
	C%	H%	C%	H%
HPP-1	62.2	5.287	62.93	4.97
HPP-2	51.25	4.759	52.25	4.59
HPP-3	47.01	4.877	46.84	4.40
HPP-4	43.02	4.728	43.58	4.29
HPP-5	40.93	4.419	41.39	4.21

Table S2 Porosity data of HPP-1-5

HPPs	Molar ratio TPE/OVS	S_{BET} / $m^2\ g^{-1}$	S_{micro} / $m^2\ g^{-1}$	V_{total} / $cm^3\ g^{-1}$	V_{micro} / $cm^3\ g^{-1}$	V_{micro} / V_{total}
HPP-1	1:0.5	1100	355	0.73	0.15	0.21
HPP-2	1:1	1540	214	1.38	0.08	0.06
HPP-3	1:1.5	1913	177	1.97	0.06	0.03
HPP-4	1:2	1438	119	1.37	0.04	0.03
HPP-5	1:2.5	1386	73	1.28	0.01	0.01

Table S3 Physical and chemical properties of dyes

Dye	Molecular sructure	Molecular size (nm)	Molecular weight (g mol^{-1})	Dye nature	UV Adsorption (nm)
CR	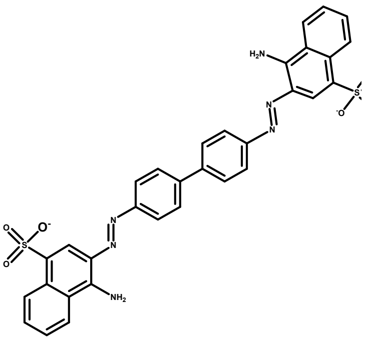	> 1.4	696	anion	497
RB	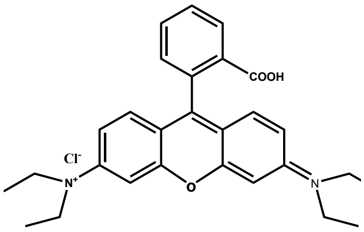	> 1.4	478	cationic	554
CV	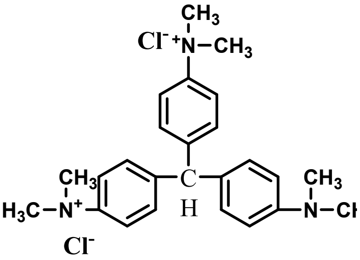	～1.4	407	cationic	586
MB	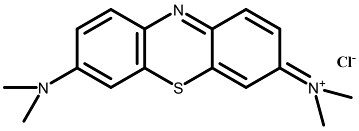	< 1.4	320	cationic	665
MO	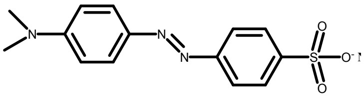	< 1.4	327	anion	466

Table S4 Kinetic parameters for the adsorption of Rhodamine B adsorption by HPP-3

Model	Parameters	
	q_{exp}(mg g^{-1})	138.8
Pseudo-first order	$q_{e,cal}$(mg g^{-1})	102.5
	k_1(min^{-1})	0.1784
	R^2	0.9711
Pseudo-second order	$q_{e,cal}$(mg g^{-1})	137.4
	k_2(g mg^{-1} min^{-1})	0.0142
	R^2	0.9997
Intraparticle diffusion	k_{i1}	26.06
	k_{i2}	0.01468

Table S5 Comparison of adsorbents of removal of Rhodamine B

Adsorbent	Physical parameter (m^2 g^{-1})	Adsorption capacity (mg g^{-1})	References
Fe3O4@POSS-SH	S_{BET}: 224	142.05	[1]
Mesoporous silica-carbon composite (MPSC)	S_{BET}: 398	281	[2]
MPSC/C	S_{BET}: 2580	785	[2]
HP-TPP-3	S_{BET}: 1105	674.6	[3]
Graphene sponge	S_{BET}: 399	72.5	[4]
SO3H-HSM	S_{BET}: 346	271	[5]
Nanoporous THPP	S_{BET}: 915	1402	[6]
HPP-3	S_{BET}: 1913	1666	This work

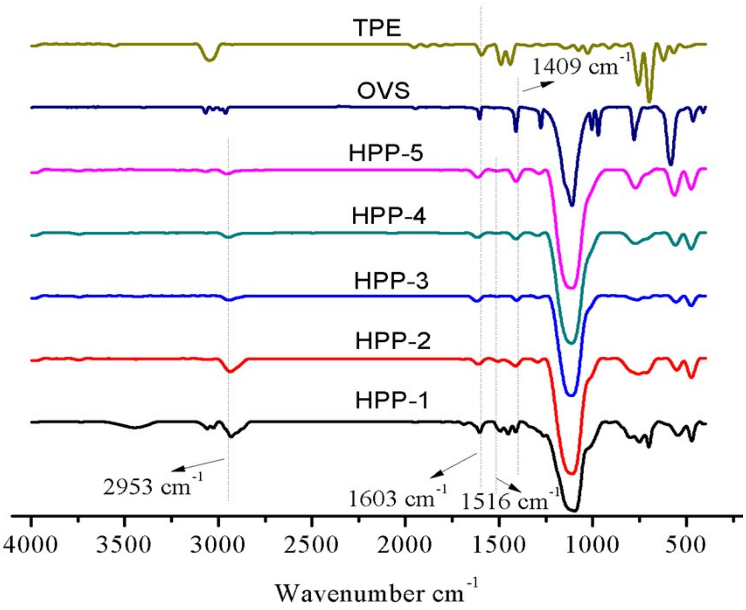

Fig. S1 FT-IR spectra of the monomers and HPPs.

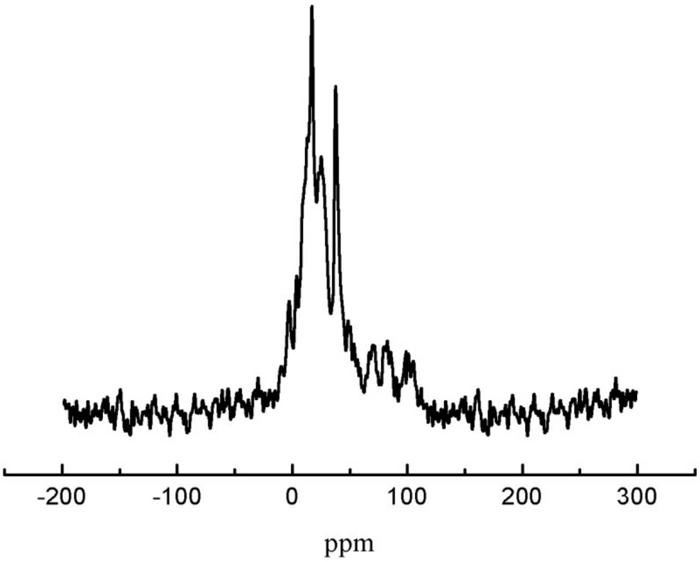

Fig. S2 Solid-state ^{13}C CP/MAS NMR spectrum of HPP-3.

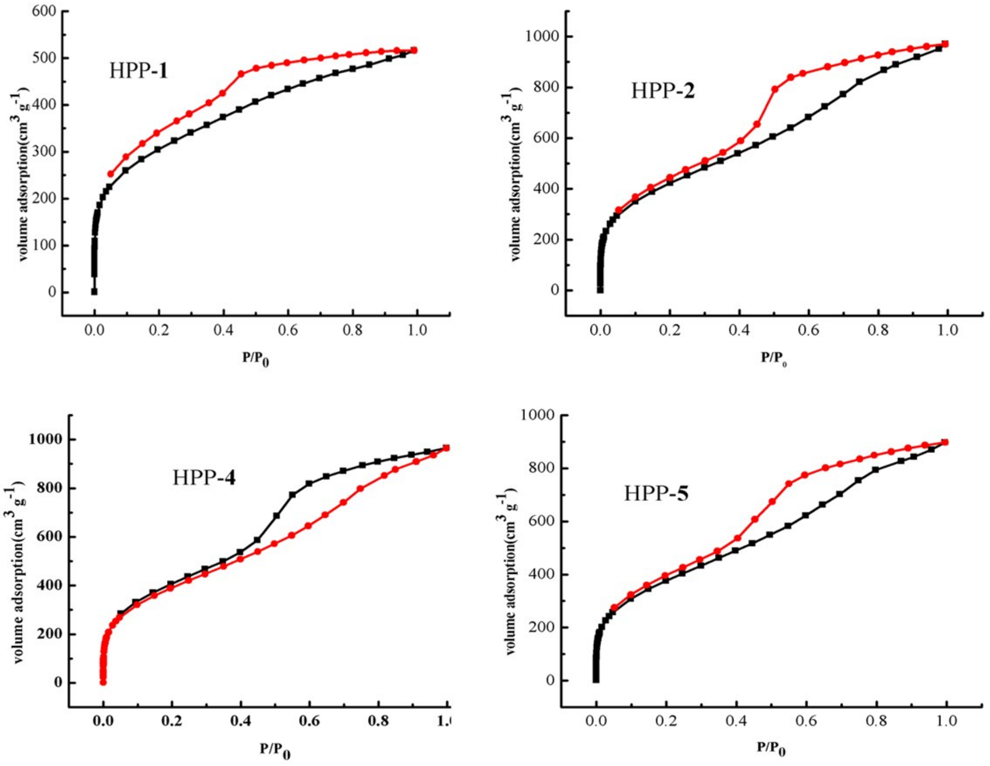

Fig. S3 N_2 sorption isotherms of HPP-**1**, HPP-2, HPP-4 and HPP-5.

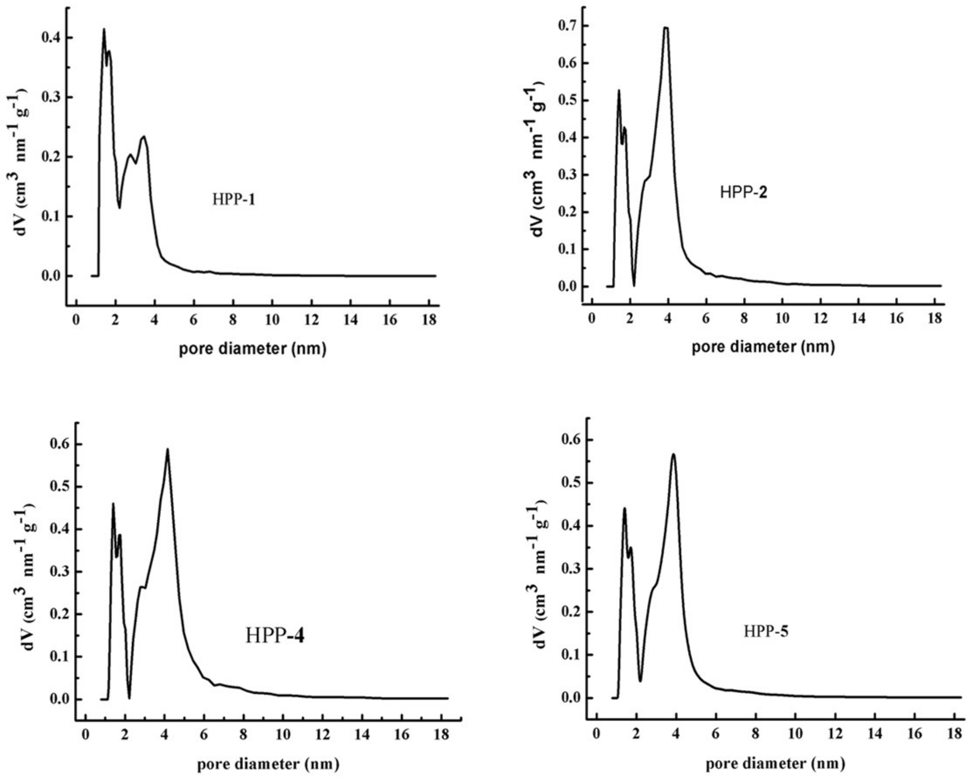

Fig. S4 NL-DFT pore-size distributions of HPP-**1**, HPP-2, HPP-4 and HPP-5.

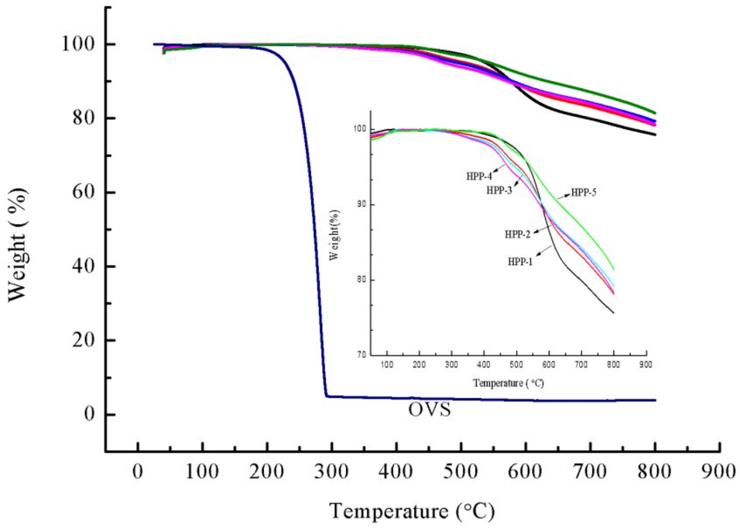

Fig. S5 TGA curves of HPP-1–5 and OVS in N_2.

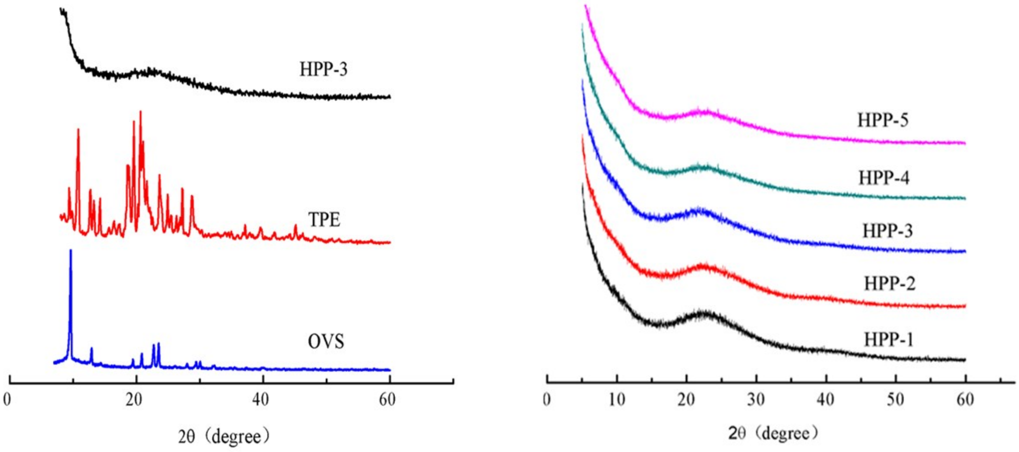

Fig. S6 PXRD patterns of HPP-1-5, OVS, and TPE: 2*θ* from 8-60°.

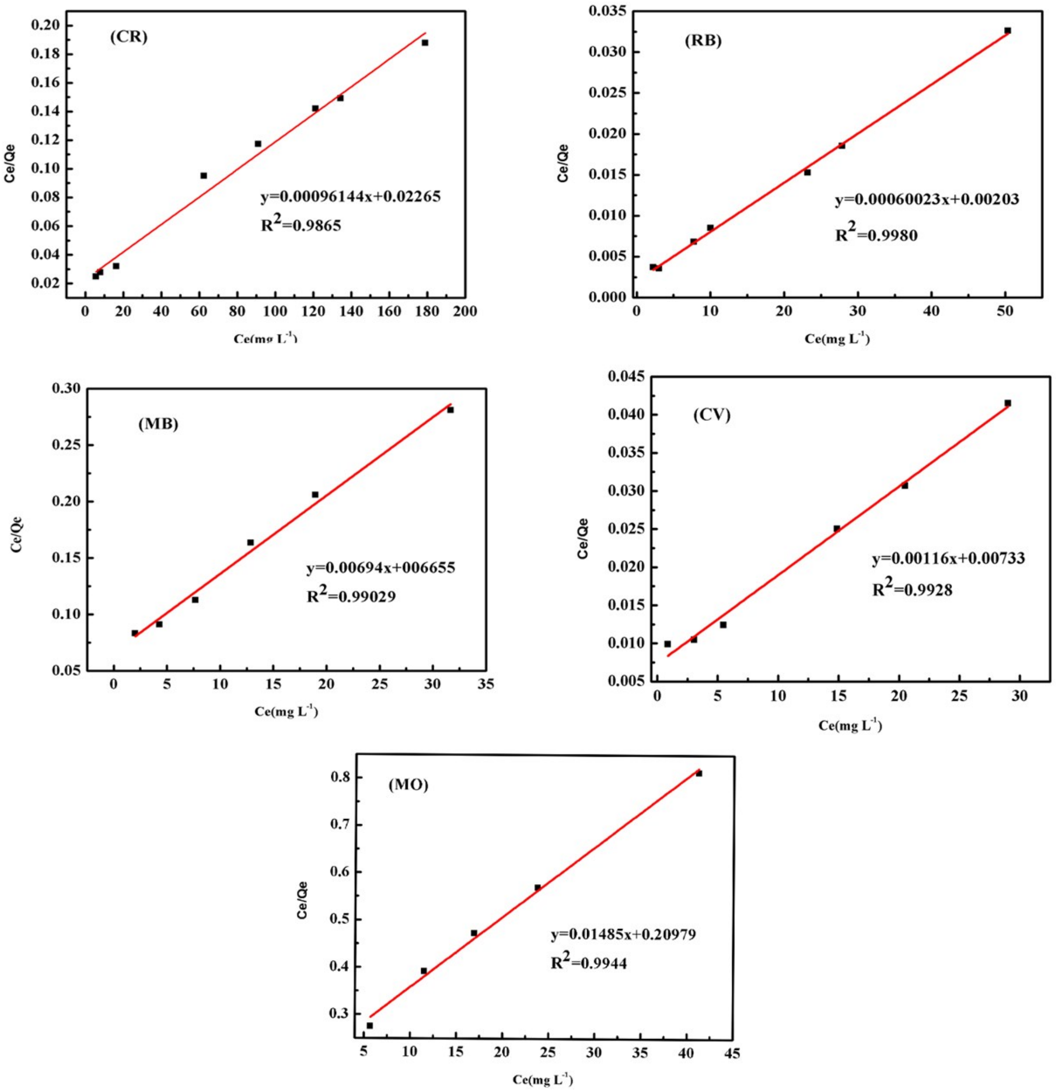

Fig. S7 The Langmuir isotherm model for RB, CR, CV, MB and MO onto HPP-3.

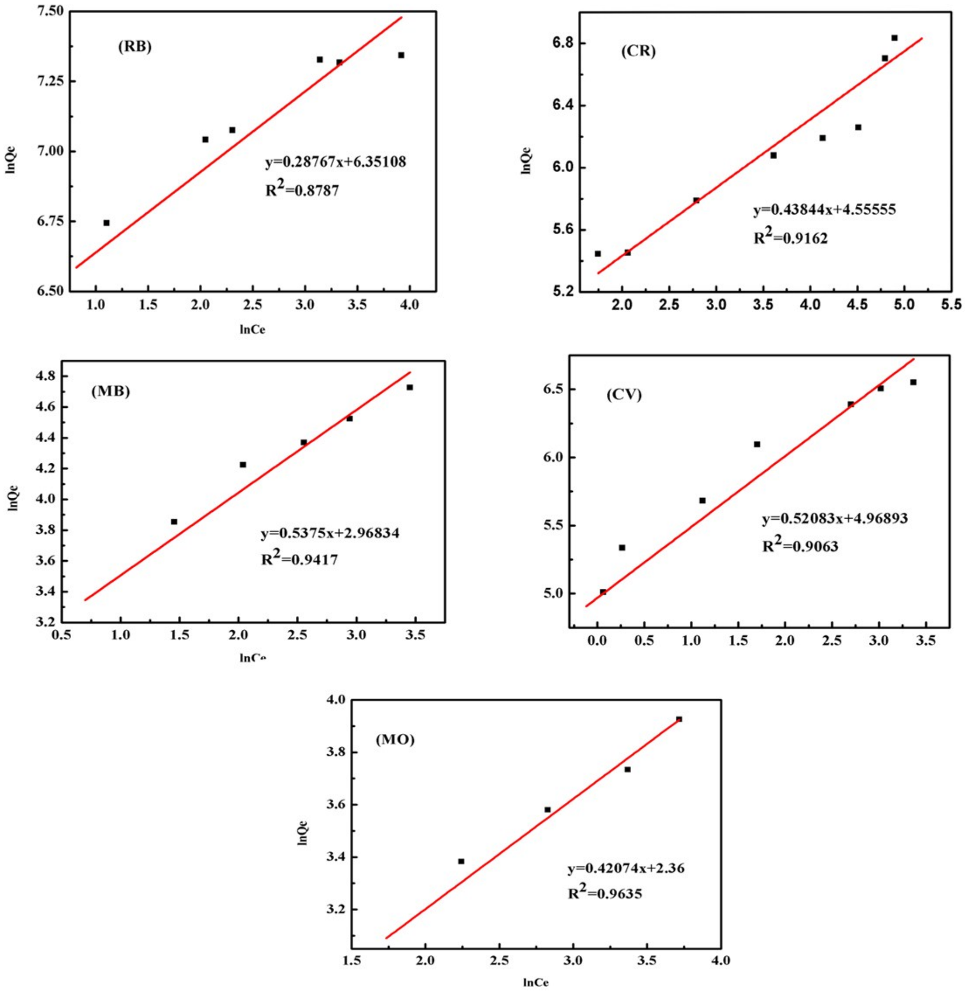

Fig. S8 The Freundlich isotherm model for RB, CR, CV, MB and MO onto HPP-3.

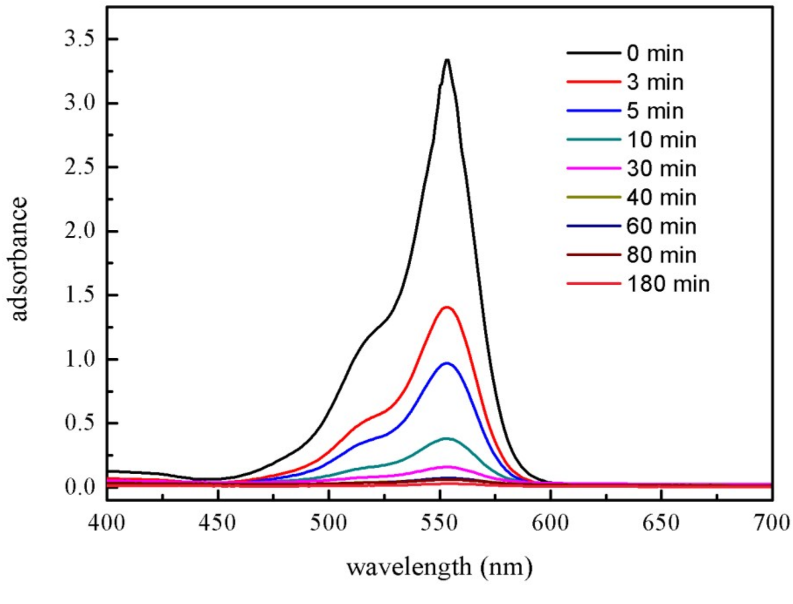

Fig. S9 UV-vis adsorption spectra of the RB solutions after being treated with HPP-3 at different time intervals.

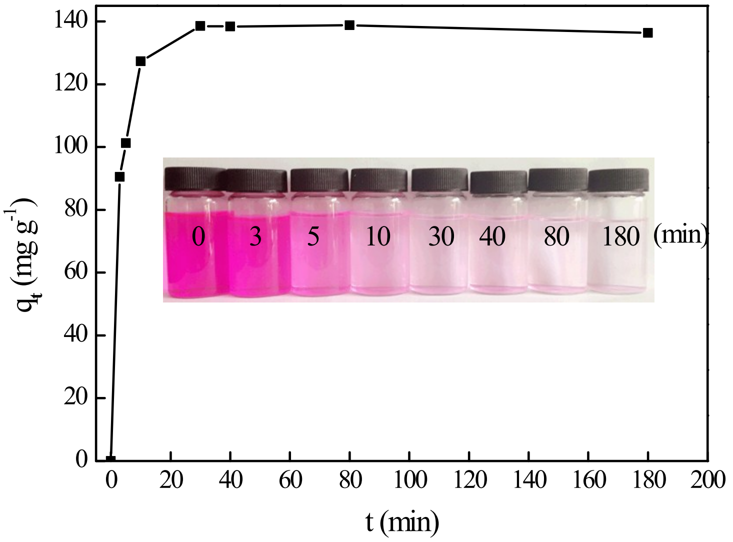

Fig. S10 Effect of contact time on the adsorption of Rhodamine B by HPP-3(inset is the photo of the dyes at 0 min and 180 min).

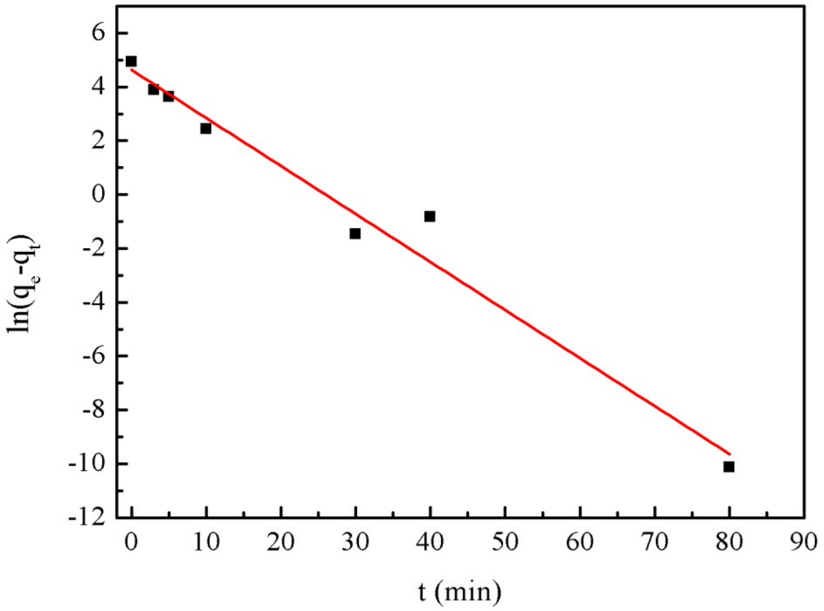

Fig. S11 The pseudo-first-order kinetic model plots for Rhodamine B adsorption by HPP-3.

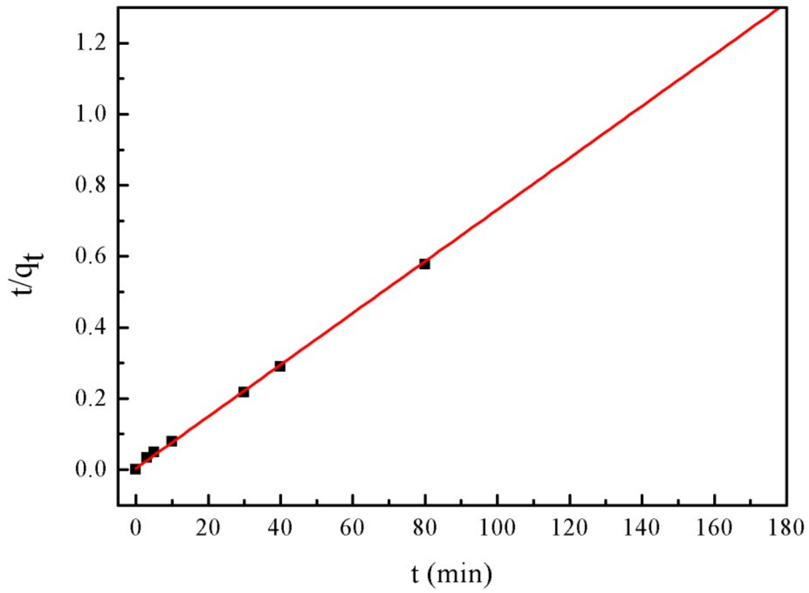

Fig. S12 The pseudo-second-order kinetic model plots for adsorption by HPP-3.

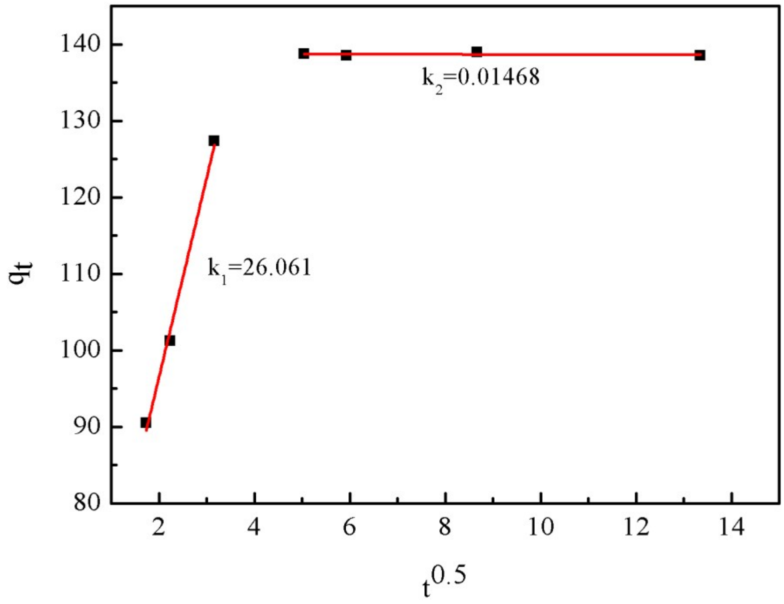

Fig. S13 The intraparticle diffusion kinetic model plots for adsorption by HPP-3.

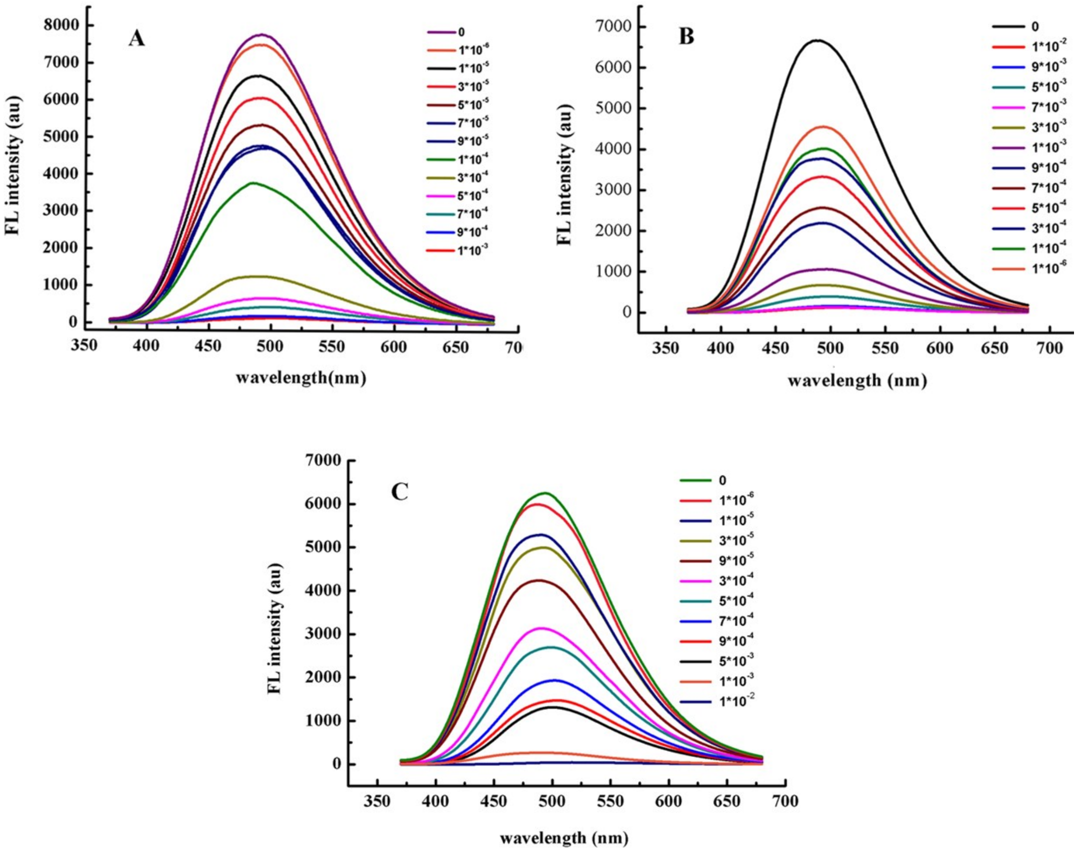

Fig. S14 Fluorescence spectra of HPP-3 upon addition of metal ion in ethanol (A) Fe^{3+}(B) Cu^{2+} (C)Ru^{3+}

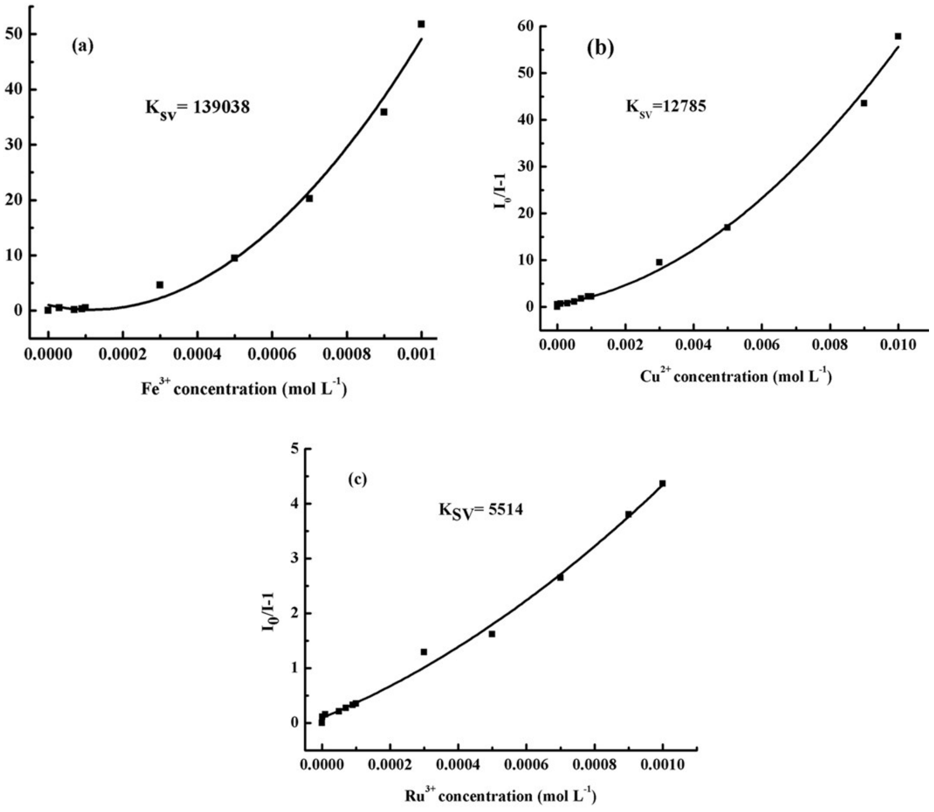

Fig. S15 Stern-Volmer plot of I_0/I-1 of HPP-3 versus [Fe^{3+}] (a), [Cu^{2+}] (b) and [Ru^{3+}] (c) and K_{SV} value.

References

1. R. J. White, V. Budarin, R. Luque, J. H. Clark and D. J. Macquarrie, *Chem. Soc. Rev.*, 2009, **38**, 3401-3418.
2. X. Zhuang, Y. Wan, C. Feng, Y. Shen and D. Zhao, *Chem. Mater.*, 2009, **21**, 706-716.
3. R. Shen and H. Liu, *RSC Adv.,* 2016, **6**, 37731-37739.
4. J. Zhao, W. Ren and H.-M. Cheng, *J. Mater. Chem.*, 2012, **22**, 20197-20202.
5. H. Furukawa and O. M. Yaghi, *J. Am. Chem. Soc.*, 2009, **131**, 8875-8883.
6. M. Ge and H. Liu, *J. Mater.Chem. A*, 2016, **4**, 16714-16722.